MRS Communications (2018), *8*, 100–106
© Materials Research Society, 2018
doi:10.1557/mrc.2018.23

MRS Communications

Research Letter

Synthetic biology with nanomaterials

Sanhita Ray and **Ahana Mukherjee,** Department of Biochemistry, University of Calcutta, 35, Ballygunge Circular Road, Kolkata-700019, West Bengal, India
Pritha Chatterjee, Department of Biochemistry and Molecular Biology, University of California at Riverside, Riverside, CA 92521, USA
Kaushik Chakraborty, Centre for Research in Nanoscience and Nanotechnology, JD 2, Sector III, Salt Lake, Kolkata-700 098, West Bengal, India
Anjan Kr Dasgupta, Department of Biochemistry, University of Calcutta, 35, Ballygunge Circular Road, Kolkata-700019, West Bengal, India

Address all correspondence to Anjan Kr Dasgupta at **adgcal@gmail.com**; **adbioc@caluniv.ac.in**

(Received 9 January 2018; accepted 13 February 2018)

Abstract

Magnetic field has been used to trigger biofilm formation. Iron oxide nanoparticles were attached to bacterial cells and cells were aggregated by application of magnetic field. Artificial cellular crowding triggered quorum sensing and led to the formation of biofilm at the sub-threshold population. Aggregation process was monitored by studying temporal dynamics of capacitance and conductance profiles. Capacitive profile exhibited a plateau upon introduction of magnetic field which was retained even after field was removed. This hysteresis property signified biofilm initiation in response to artificial crowding. This work demonstrates how synthetic biology is enabled by including nanoparticles in the interactome.

Introduction

Synthetic biology[1,2] has been viewed till now as the prerogative of molecular systems biologists and geneticists. Most work in this field has involved creation of an artificial genetic network and housing it inside a single cell. A major aim in synthetic biology is to control the expression from this circuitry by means of external stimuli. Cellular computational processes have been achieved but only within a single cell. Synthetic approaches have never been used to investigate emergent (nonlinear) output at the population level.

The simplest example of population-based computing is bacterial quorum sensing (QS).[3] QS is a response[4] to cellular crowding. Such crowding occurs upon cell division and population increase. Microbial crowding and consequent QS give rise to a number of physiological changes in the population, for example, bioluminescence in *Vibrio fisheri*, and virulence gene expression in virulent species. One well-studied consequence of QS is biofilm formation[5,6] initiation. Quorum threshold crossing has been observed in single bacterium kept in a microfluidic well.[7] These authors have introduced the idea of "bacterium in a box" which bears some parallel with the present work. This inspired the present concept that, even without cell growth, we may achieve increased local cell density by pulling the cells together.

Super-paramagnetic iron oxide nanoparticles (SPIONs)[8–12] can be aggregated by application of the static magnetic field.[11] The underlying strategy is to attach suitably functionalized SPIONs to target cells. Cellular aggregation is due to the application of magnetic field to SPION-coated cells. SPION-mediated bacterial aggregation has been previously used for bacterial detoxification of oil spill.[13] Other applications include cell patterning in two-dimensional (2D) or 3D templates.

Electrical measurement using interdigitated electrodes (IDE) have been previously used for electrochemical impedance spectroscopy (EIS) to detect and characterize[14] biofilms. Capacitive measurements have been used previously to detect the presence of specific microbes as well as biofilm formation.[15,16] We explore artificial manipulation of population-level computing[4] to give biologic output (e.g., protein expression) at desired instances. Instead of genetic engineering, we use material science[8,9] as a toolbox to achieve crowd-level response manipulation.

Our aim is to quantify, as well as monitor in real time, biofilm formation caused by artificial, magnetic field-assisted cellular crowding. The present work deals with SPION and static magnetic field-induced bacterial aggregation and consequent biofilm formation.

Materials and methods

SPION synthesis and functionalization

Since bacterial cell outer membranes are negatively charged, SPIONs with large positive charges are necessary to bind them. (3-Aminopropyl) triethoxysilane (APTES), when treated with mild acidic solution, acquires a positive charge due to its NH_2 group.[17] In addition, APTES possesses an *n*-propyl group which is expected to give some maneuverability to APTES functionalized SPIONs which get attached to bacterial cell surfaces.

Bare SPION synthesis

$FeCl_3$ and $FeCl_2$ were taken in 2:1 ratio in an acidic solution of pH 2 and stirred in anoxic condition. NaOH (1 M) was added to

https://doi.org/10.1557/mrc.2018.23 Published online by Cambridge University Press

the salt solution to bring about the quick transition at pH 10, under nitrogen purging. The stirring was allowed to continue for some time and resulted in the formation of a black precipitate. The precipitate was washed by magnetic decantation from water and suspended in methanol.

Functionalization

The methanolic suspension was sonicated in bath sonicator and heated to 90 °C in order to reach boiling temperature of methanol. Repeated addition and boiling off of methanol was used to get rid of residual water. The anhydrous condition is required for efficient APTES attachment to SPION. Next, the temperature was lowered to 60 °C, and 30 mL toluene was added to 40 mL methanolic suspensions of SPION. 3 mL APTES was added and stirring was allowed to continue at 60 °C for 4 h.

The dispersed suspension was washed repeatedly with magnetic decantation from methanol. 2 mL of 12 N HCl was added to a methanolic suspension of APTES–SPION for charging the amino group in APTES. Particles were magnetically separated from methanol and re-suspended in milliQ water and washed with milliQ.

Characterization

Characterization of the SPION was done with Malvern Zetasizer (Model NanoZS, UK).

DLS and zeta potential measurements were done by suspending particles at pH 2, 4, and 5. pH of the suspension was adjusted by adding 2 N HCl drop by drop and using pH paper for measuring pH.

Bacterial growth

Rhodobacter capsulatus was used as model microbe due to stable capacitance signals obtained from their biofilms. *Rhodobacter* strain was kindly provided by Dr. Patrick Hallenbach of University of Montreal, Canada. *Rhodobacter* was grown in the RCV medium[18] in the presence of light and in anaerobic condition.

Artificial crowding

SPION was mixed with *R. capsulatus* liquid culture in ratios of 1:1, 2:8, 3:7, and 4:6. The mixtures were kept upright and magnet of 0.45 T was kept parallel to the container surface; see Fig. 1(I). Cellular aggregation was observed in the vicinity of the magnet and the rest of the liquid turned clear (see Fig. S1).

The synthesized SPIONs in acidic medium pH 2 were charged to such an extent that due to Coulombic repulsion they resisted aggregation on the application of 0.45 T. However, on admixture with bacterial cells their zeta potential decreased significantly [see Fig. 1(II) (c and d)] and aggregation could be achieved by application of the static magnetic field. Cellular aggregation was reversible as shown in Fig. S1(A).

However, each SPION–bacteria mixture had different aggregation kinetics. Kinetics of cellular aggregation was measured by monitoring change in capacitance and resistance values with time.

Electrical measurements

To achieve toggle control of a quorum-controlled circuitry, it is necessary to monitor the aggregation process itself. For low cell densities which are required for this work, sensitive monitoring is difficult and expensive. However, capacitance and conductivity-based sensing can be achieved cheaply.

Open hardware-based system was used to measure the di-electric constant in the form of capacitance using IDEs. Hence, the dimension of IDE was same in all experiments and the dielectric constant is monitored by measuring the capacitance. Capacitance measurement was done by a single reconfigurable open hardware setup[19] (Arduino Nano) where data logging is possible.

IDEs were purchased from commercial manufacturers Dropsens (IDEAU10) having cell constant = 0.0118/cm, a number of digits: 125 × 2, a digit length = 6.76 mm, and gap 10 μm. This arrangement was important to achieve sufficient current for measurement.

The static magnetic field was applied in the area very close to the IDE surface so that SPION-coated cells aggregated on the surface of IDEs [see Figs. 2(a) and 2(b)], forming a thick layer on the electrode surface. Capacitance decay was monitored for (a) only SPION solution, (b) only bacterial suspension, and (c) for various ratios of SPION and bacteria. Capacitance monitoring was done by the time-constant method.[20]

Resistance measurement of bacteria–SPION suspensions were carried out with DC voltage in the presence and the absence of magnetic field. These measurements were performed using Arduino Uno.

Biofilm assay on enzyme-linked immunosorbent assay (ELISA) plate

Biofilm formation due to artificial cellular aggregation was studied by taking a suspension of SPION-coated RCSB (on the second day of growth) in ELISA plate wells. Rare-earth magnet (0.45 T) was placed below wells in a row. Similarly filled row at another end of the plate was taken as control. Two other rows near the magnet were also filled with suspension. Plates were wrapped in cling film to maintain anaerobic condition and placed on the magnet in presence of light at room temperature. After 2 h of the magnetic field-driven cellular aggregation, the plates were washed thoroughly with 10 mM phosphate buffer in order to remove any planktonic cells. Subsequently, all wells were treated with methanol and stained with Acridine orange (AO). Amount of AO absorbed was quantitated by using a BIO-RAD iMark microplate reader. This gives an indication of DNA in each well. Biomass in each well was quantitated by staining with 0.1% crystal violet (CV) and further washing with milliQ water. Absorbed CV was measured in a microplate reader at 595 nm.

AO-stained wells were imaged using confocal microscopy (inverted confocal microscope Olympus, FV 1000) with a

https://doi.org/10.1557/mrc.2018.23 Published online by Cambridge University Press

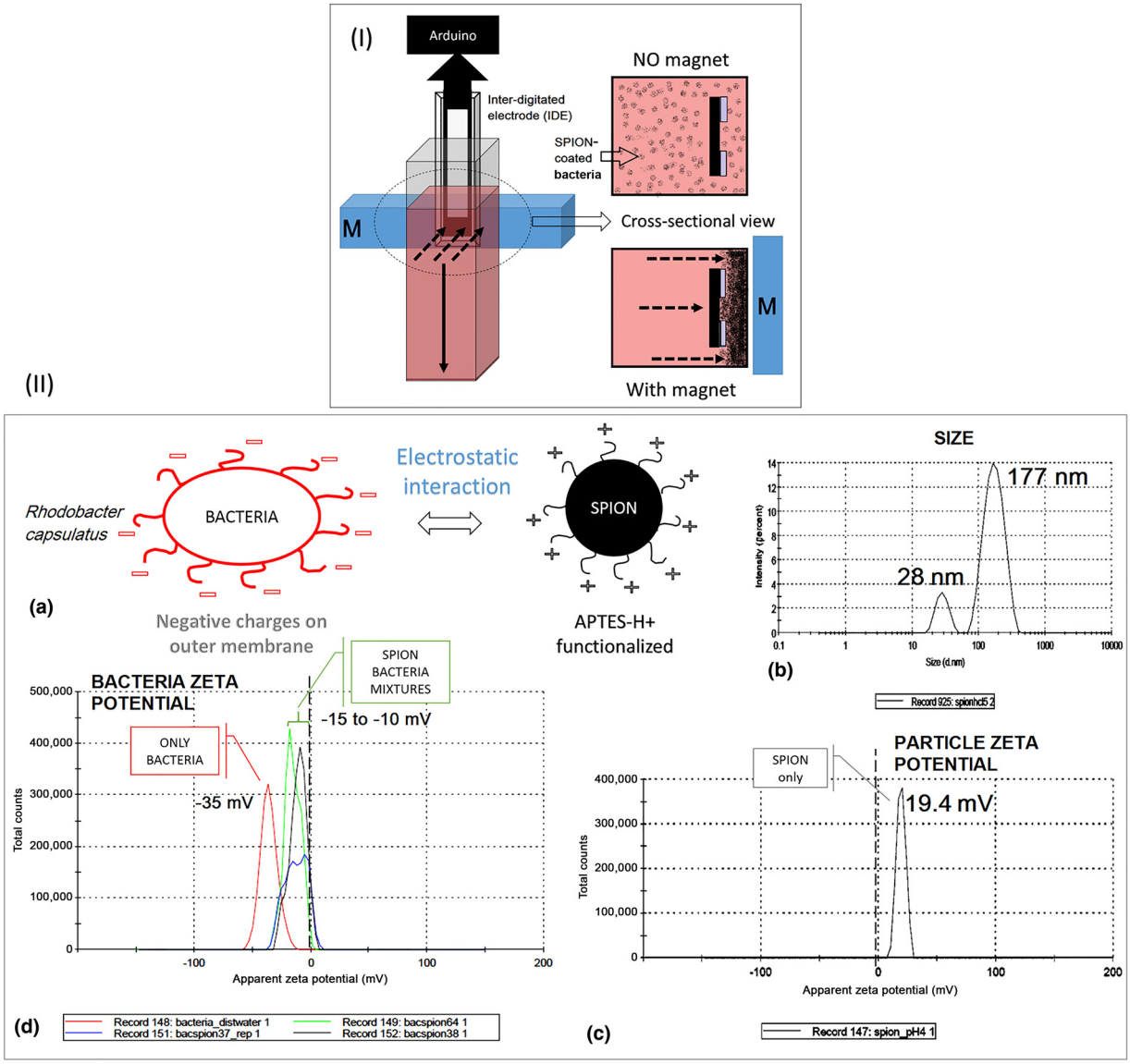


Figure 1. (I) Setup for electrical monitoring of artificial aggregation. Schematic representation showing setup and direction of magnetic field with respect to the interdigitated electrode. (II) (a) Attachment of APTES-H + coated SPIONs to negatively charged bacterial surface. (b) Hydrodynamic radius and (c) Zeta potential of APTES-H + coated SPIONs (d) Zeta potential of control bacterial cell compared to that of SPION-coated bacterial cells.

green filter. *Z*-scanning was performed and obtained images were stacked. This process ensured proper imaging of extracellular matrix. The matrix contains secreted DNA, hence expected to take up AO which is a nucleic acid stain. Due to well bottom thickness, measurements could only be done with 10 × magnification objective lens.

Results

SPION characterization

Size

Dynamic light scattering (DLS) revealed a mixture of two populations, diameter = 177 nm and 28 nm, PDI = 0.286 [see Fig. 1(II) (b)]. The larger particles were approximately twice the size of the smaller particles, indicating cross-linking mediated by APTES.

Zeta potential

Particles showed a positive zeta potential of 19.4 mV at pH = 2. The high value of surface potential indicates stable particle at low pH. However, increase in pH led to falling in surface potential.

Bacteria–SPION interaction

Bacterial interaction with SPION was characterized by measuring bacteria–SPION mixtures at various ratios. Bacterial cells showed a high negative zeta potential (−35 mV). However, upon SPION addition the value shifted toward lesser negative

https://doi.org/10.1557/mrc.2018.23 Published online by Cambridge University Press

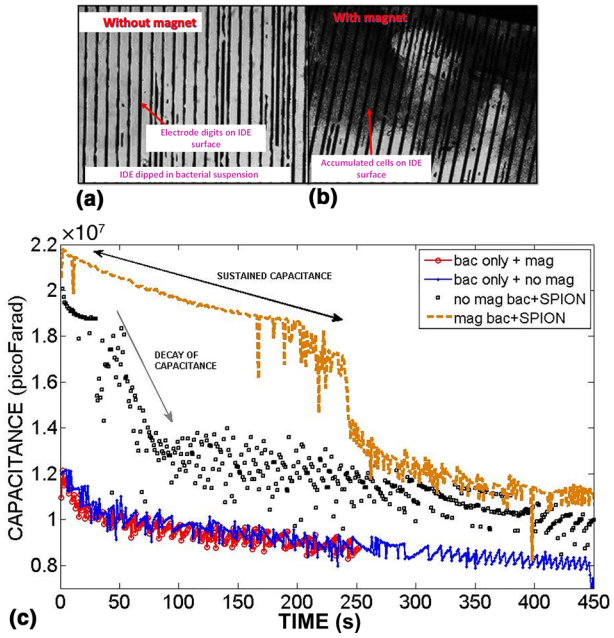


Figure 2. (a) Light microscopic image of interdigitated electrode surface after immersion in bacteria–SPION suspension. In the suspension, same numbers of SPION-coated bacterial cells were added. The surface density of bacterial population significantly differs in the absence (a) and in the presence (b), of static magnetic field (0.45 T), to attract the SPION-conjugated bacteria. (c) Real-time capacitance change of SPION–bacteria with and without magnetic fields.

values (−15 to −10 mV). Therefore SPION and bacteria neutralize each other's zeta potential. This implies stable binding between cell and SPION due to electrostatic interaction [see Fig. 1(II) (c) and (d)]. Real-time capacitance monitoring was used to determine the ideal stoichiometry.

Aggregation experiments

When the magnetic field was applied to SPION-coated bacteria, the cells crowded together (see Supplementary Fig. S1) near the cuvette wall closest to a magnet. Due to the placement of electrodes, SPION-coated bacterial cells formed a thick layer on the IDE surface [see Figs. 2(a) and 2(b]. Such cellular crowding was expected to change the capacitance value across the electrode pair since effective dielectric constant of the intervening medium is changed.

Aggregation [see Figs. 2(a) and 2(b)] was monitored by real-time capacitance measurement. Uncoated bacterial cells, uniformly suspended in the growth medium, showed a bi-exponential decay in their capacitance time-series. This pattern was unaffected upon application of magnetic field. SPION-coated cells showed same exponential decay pattern, though the exponents had different values. On application of magnetic field, an initial period of sustained capacitance [see Fig. 2(c)] was observed for SPION-coated bacterial cells and this corresponds with cellular aggregation as shown in Fig. 2(a). We refer to this period as the capacitance plateau. The capacitance plateau lasted over a certain time period depending on SPION: bacteria ratio, bacterial density, days of growth of the bacterial suspension used (see Supplementary Fig. S2). If observed for long enough time, in some cases, the capacitance plateau was followed by bi-exponential decay. Capacitance plateau is explained as follows. When bacterial cells are uniformly suspended, ions in bacterial growth media have access to IDE surface. Such mobile charge carriers dissipate charge stored across the electrodes. This dissipative/leakage current corresponds to the bi-exponential decay phase. However, when there is cellular crowding on the IDE surface, ions are excluded (see Supplementary Fig. S3) from the vicinity of the electrodes, and hence no leakage current is generated. Bacterial cells being very good dielectrics gives rise to high, sustained value of capacitance. The eventual decay in some cases is probably due to slow diffusion of ions through the cellular milieu.

Memory

Aggregation process studied above is not the ultimate aim of this study. Our aim was to demonstrate that artificial aggregation triggers the expression of cellular function by a remote manipulation. Specifically, our target, in this case, is to observe synthetic biofilm formation in response to artificial crowding. Studying capacitance time-series after removal of magnet and re-suspension of aggregated cells provided proof of synthetic biofilm initiation.

The capacitive device retained the memory of magnetic field induced aggregation. Capacitance values showed sustained plateau when the magnetic field was applied and subsequently withdrawn [see Fig. 3(I) trace 3]. The sustained plateau was present even when the magnet was removed and aggregated cells were re-suspended. We refer to this as a memory phenomenon since it is normally expected that upon withdrawal of magnetic field, capacitive time-series would be identical to what it was before application of the field. However, the experiment shows that in this case there is no such perfect reversibility. It is noted here that this has some parallel to hysteresis shown during the magnetization/de-magnetization cycle for ferromagnetic materials, though hysteresis is absent in SPIONs.

Capacitance plateau obtained after the dispersal of a visible thick layer on IDE signifies that some bacterial cells have seeded on the IDE surface and biofilm initiation (with the probable secretion of extracellular matrix) has occurred. This nascent biofilm is probably one/two cell layers thick and thus invisible to the naked eye.

Resistance study

Real-time monitoring of resistance in the presence of magnetic field showed a change in mean value with field and after removal of the field, when compared with mean value before application of the field. However, these effects were dependent on SPION–bacteria ratio (see Fig. S4). For SPION-to-bacteria ratio of 3:7, the introduction of magnetic field increased resistance values [see Fig. 3(II) (a)].

When the field was withdrawn, resistance values showed further increase.

https://doi.org/10.1557/mrc.2018.23 Published online by Cambridge University Press

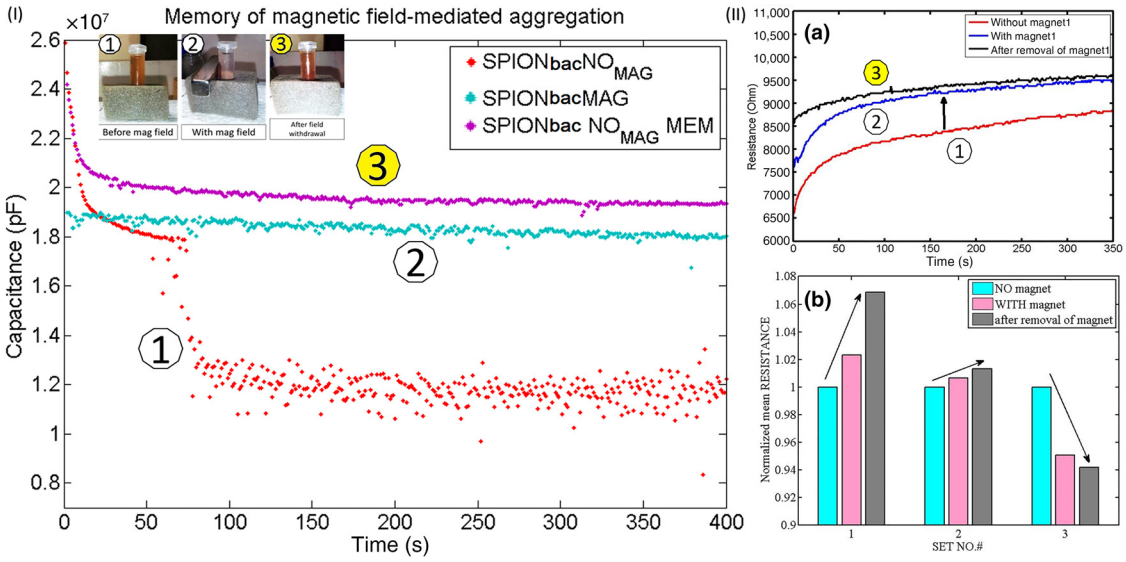


Figure 3. (I) Memory of the capacitive system for magnetic aggregation. Capacitance time-series was measured without magnet (1), in the presence of magnet (2), and immediately after removal of the magnet (3). Correlate these states (1, 2, and 3) with that in Fig. 1(b) (II). (a) Resistance time-series of bacteria–SPION suspension in the absence and presence of magnetic field and after removal of the magnetic field. (b) Normalized resistance values with respect to "no magnet" show that for successive sets the tendency to increase is flattened and ultimately reversed.

Upon repeating the aggregation–de-aggregation experiment with the same IDE thrice, a gradual shift in resistance change was obtained [see Fig. 3(II) (b)]. For the second set, the lesser increase was observed (i.e., a flattened response was obtained). For the third set, resistance values decreased upon application of the field. This may be regarded as a class of memory (like the dielectric memory referred above) whose presence is realized by irreversible changes in conductance. The lowering of resistance values (in response to the introduction of static magnetic field) may be explained as follows: with repeated cycles of cell seeding, bacterial percolation occurred between the electrode pair. Since *Rhodobacter* is a photon-capturing microbe, it has an elaborate network of electron carriers on its surface which transports energy absorbed from the incident photon. It is possible that lowering of resistance values is due to the passage of electrons through electron transporter chain. We take hysteresis to be the difference between resistance after removal of the magnet and what it was initially, that is before application of the field. This difference may be used as a metric of how much biofilm initiation has occurred. Thus for ratio 3:7, highest hysteresis was observed (see Supplementary Fig. S4). For the higher proportion of bacteria relative to SPION, resistance values decreased upon cellular aggregation. After removal of the magnetic field, the resistance increased but did not regain original values. Hence, in these cases (8 : 2 and 9 : 1), hysteresis was present but much lower. The lowering of resistance value can be explained, as before, in terms of electron percolation between the electrodes.

Validation of synthetic formation of biofilm

Synthetic biofilms were formed on the bottoms of ELISA plate wells [see Fig. 4(a)], by a magnetic field-induced aggregation of cells. AO staining revealed higher stain retention by wells where aggregation occurred in response to the field, compared with control wells [see Fig. 4(b)]. CV staining assay was used to quantitate biofilm biomass formation. CV staining showed significantly more stain retention for biofilm formed due to a magnetic field-assisted aggregation [see Fig. 4(c)]. Microscopic observation of AO-stained wells revealed thick uniform adherent biofilm on the bottom of wells placed above magnet [see Fig. 4(e)]. For control wells [see Fig. 4 (d)], precipitated cell clumps were observed by microscopy, which may have led to nascent biofilm formation. Such discontinuous nascent biofilm may have led to the non-zero CV staining of control wells.

Discussions

Artificial crowding changes percolation status

Any threshold response may be modeled as a process of percolation (see Supplementary Fig. S5, in which we have described a simple lattice model to achieve percolation behavior, the probability of percolation being plotted against the probability of obtaining a percolating cluster). QS threshold is determined by bacterial cell density in a particular niche. If we decrease the total volume under consideration, then we may get ON signal even for sub-quorum densities (bearing some parallel with the work of Hagen et al.[7]) This process of volume constriction may be achieved by local crowding.

We have simulated 2D biofilm formation (run the function biofilm_mag.m hosted on https://drive.google.com/open?id=16brYLc5THn8RlYcOMhwricyyJZR3fkJC) through a lattice model that is somewhat similar to the percolation experiment in Fig. S5. We have taken the growth rate to be proportional to

https://doi.org/10.1557/mrc.2018.23 Published online by Cambridge University Press

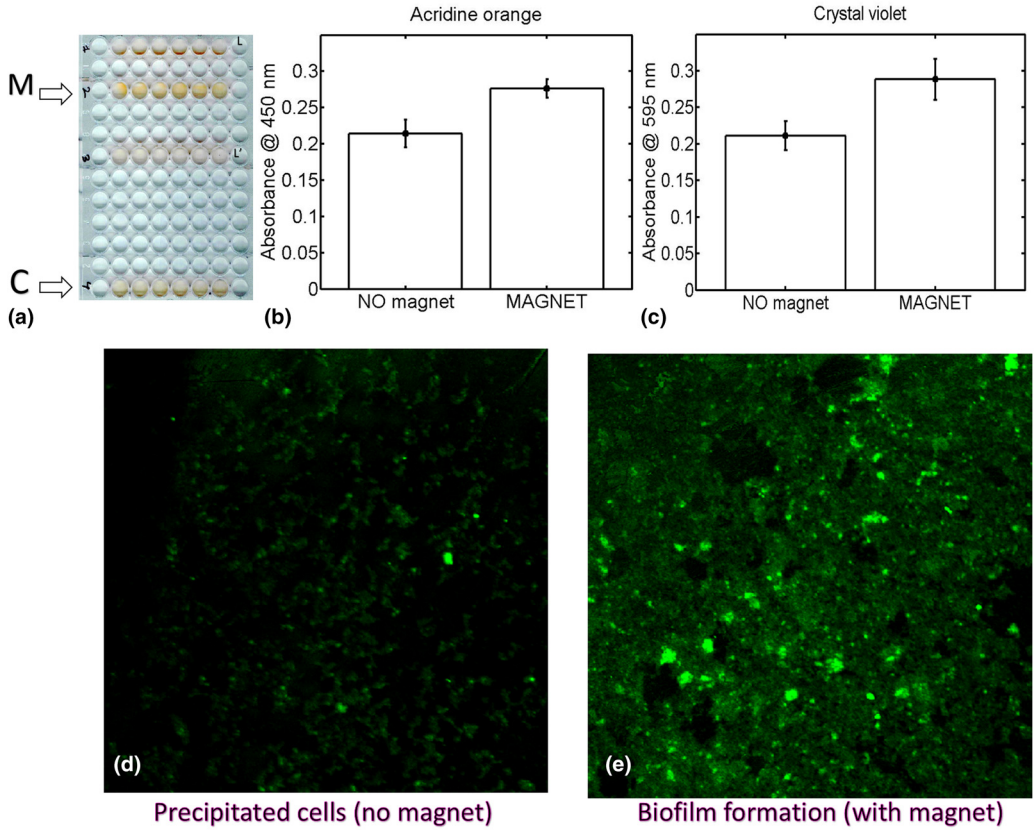


Figure 4. (a) SPION incorporated biofilm formation (M) in the ELISA plate bottom in response to application of magnetic field, C denotes control, i.e. where no magnetic field was present. (b) Acridine orange absorbance at 450 nm and (c) crystal violet absorbance, obtained with ELISA plate reader, for +magnet and no magnet. (d, e) Fluorescence microscopic images of Acridine-stained ELISA plate wells showing cell clumps in the absence of magnetic field and biofilm formation in the presence of magnetic field.

the average distance between seed cells (thus mimicking QS). We have engineered a bias in the initial distribution such that seed cells (at time t_0) occupy only a small percentage of the total area available for growth. This is similar to cellular crowding that is achieved through magnetic pulling experiment. Our biofilm growth model shows that apparent carrying capacity (K_{app}) is decreased (see Supplementary Fig. S6) when the initial bias conditions are turned ON, compared with when initial seeding occurs at random over the whole surface. However, we know that space for growth is actually same in both cases. Hence, a decrease in K_{app} must signify that the peak growth rate occurs for the lesser population than before. This demonstrates how artificial QS changes cellular computation or decision-making processes.

Applications

Multiple methods of studying magnetic field-induced cellular aggregation and biofilm initiation have been explored in order to obtain multiple parameter-based monitoring of this process. They can be used to study microbe-based materials (e.g., living sensor) fabrication on device surfaces. Additionally, the whole process may be miniaturized on a microfluidic device to obtain a lab-on-chip approach toward detecting rare bacterial cells or micron range suspended biofilm in a water sample. This technology provides us means to control a microbial population according to need and may supplement 2D or 3D printing approaches. A combinatorial biomaterials approach is possible where SPION-coated bacteria are mixed with suspended graphene and are artificially aggregated to form a graphene incorporated, synthetic, and conductive, biofilm. Use of open hardware technology means that this process can be easily integrated into robotics-based approaches for fabricating green devices.

Conclusion

In this work, the magnetic field has been used to trigger biofilm formation. Magnetic field-assisted cellular crowding can be monitored in real time by studying capacitance and resistance time-series. Magnetic field-induced synthetic cellular crowding can be tuned by changing the SPION–bacteria ratio. Capacitive device retained the memory of magnetic field-driven aggregation. The memory of electrical changes even after field removal implied enhanced biofilm initiation. Synthetic biofilm formation can be monitored in real time by studying hysteresis in capacitance and resistance changes. The effect can be modeled by apparent reduction of carrying capacity in a logistic framework.

https://doi.org/10.1557/mrc.2018.23 Published online by Cambridge University Press

Supplementary material

The supplementary material for this article can be found at https://doi.org/10.1557/mrc.2018.23

Acknowledgments

This work was supported by the Department of Biotechnology (BT/PR3957/NNT/28/659/2013), India. S.R. thanks CSIR-India for Senior Research Fellowship [Sanction no. 09/(028)0875]. This work has been chosen for oral presentation at MRS Fall Meeting 2017, for which travel support is being provided by the ITS–SERB scheme of the Department of Science and Technology, India.

References

1. P. Oldham, S. Hall, and G. Burton: Synthetic biology: mapping the scientific landscape. *PLoS ONE* **7**, e34368 (2012).
2. M.C. Jewett, K.A. Calhoun, A. Voloshin, J.J. Wuu, and J.R. Swartz: An integrated cell-free metabolic platform for protein production and synthetic biology. *Mol. Syst. Biol.* **4**, 220 (2008).
3. C.A. Brimacombe, A. Stevens, D. Jun, R. Mercer, A.S. Lang, and J.T. Beatty: Quorum-sensing regulation of a capsular polysaccharide receptor for the *Rhodobacter capsulatus* gene transfer agent (rcgta). *Mol. Microbiol.* **87**, 802–817 (2013).
4. M.R. Parsek and E. Greenberg: Sociomicrobiology: the connections between quorum sensing and biofilms. *Trends Microbiol.* **13**, 27–33 (2005).
5. J. Zhu and J.J. Mekalanos: Quorum sensing-dependent biofilms enhance colonization in vibrio cholera. *Dev. Cell* **5**, 647–656 (2003).
6. G. O'Toole, H.B. Kaplan, and R. Kolter: Biofilm formation as microbial development. *Annu. Rev. Microbiol.* **54**, 49–79 (2000).
7. S.J. Hagen, M. Son, J.T. Weiss, and J.H. Young: Bacterium in a box: sensing of quorum and environment by the luxi/luxr gene regulatory circuit. *J. Biol. Phys.* **36**, 317–327 (2010).
8. J. Borcherding, J. Baltrusaitis, H. Chen, L. Stebounova, C.-M. Wu, G. Rubasinghege, I.A. Mudunkotuwa, J.C. Caraballo, J. Zabner, V. H. Grassian, and A.P. Comellas: Iron oxide nanoparticles induce *Pseudomonas aeruginosa* growth, induce biofilm formation, and inhibit antimicrobial peptide function. *Environ. Sci. Nano* **1**, 123–132 (2014).
9. C. Haney, J.J. Rowe, and J.B. Robinson: Spions increase biofilm formation by *Pseudomonas aeruginosa*. *J. Biomater. Nanobiotechnol.* **3**, 508 (2012).
10. H. Zolata, F.A. Davani, and H. Afarideh: Synthesis, characterization and theranostic evaluation of indium-111 labelled multifunctional superparamagnetic iron oxide nanoparticles. *Nucl. Med. Biol.* **42**, 164–170 (2015).
11. H. Maleki, A. Simchi, M. Imani, and B. Costa: Size-controlled synthesis of superparamagnetic iron oxide nanoparticles and their surface coating by gold for biomedical applications. *J. Magn. Magn. Mater.* **324**, 3997–4005 (2012).
12. U. Sakulkhu, M. Mahmoudi, L. Maurizi, G. Coullerez, M. Hofmann-Amtenbrink, M. Vries, M. Motazacker, F. Rezaee, and H. Hofmann: Significance of surface charge and shell material of superparamagnetic iron oxide nanoparticle (spion) based core/shell nanoparticles on the composition of the protein corona. *Biomater. Sci.* **3**, 265–278 (2015).
13. Y.-G. Li, H.-S. Gao, W.-L. Li, J.-M. Xing, and H.-Z. Liu: In situ magnetic separation and immobilization of dibenzothiophene-desulfurizing bacteria. *Bioresour. Technol.* **100**, 5092–5096 (2009).
14. A.P. Borole, D. Aaron, C.Y. Hamilton, and C. Tsouris: Understanding long-term changes in microbial fuel cell performance using electrochemical impedance spectroscopy. *Environ. Sci. Technol.* **44**, 2740–2745 (2010).
15. T. Kim, J. Kang, J.-H. Lee, and J. Yoon: Influence of attached bacteria and biofilm on double layer capacitance during biofilm monitoring by electrochemical impedance spectroscopy. *Water Res.* **45**, 4615–4622 (2011).
16. R. Mauricio, C. Dias, and F. Santana: Monitoring biofilm thickness using a non-destructive, on-line, electrical capacitance technique. *Environ. Monit. Assess.* **119**, 599–607 (2006).
17. Y. Liu, Y. Li, X.-M. Li, and T. He: Kinetics of (3-aminopropyl) triethoxylsilane (aptes) silanization of superparamagnetic iron oxide nanoparticles. *Langmuir* **29**, 15275–15282 (2013).
18. M. Leclerc, A. Colbeau, B. Cauvin, and P.M. Vignais: Cloning and sequencing of the genes encoding the large and the small subunits of the h 2 uptake hydrogenase (hup) of *Rhodobacter capsulatus*. *Mol. Gen. Genet. MGG* **214**, 97–107 (1988).
19. Y.A. Badamasi: The working principle of an Arduino, in: IEEE 2014 11th Int. Conf. on Electronics, Computer and Computation (ICECCO). , 2014, pp. 1–4.
20. B. Hirschorn, M.E. Orazem, B. Tribollet, V. Vivier, I. Frateur, and M. Musiani: Determination of effective capacitance and film thickness from constant-phase-element parameters. *Electrochim. Acta* **55**, 6218–6227 (2010).

https://doi.org/10.1557/mrc.2018.23 Published online by Cambridge University Press